CHEMISTRY OF MATERIALS

pubs.acs.org/cm

Article

Hydrophobic Association Hydrogel Enabled by Multiple Noncovalent Interactions for Wearable Bioelectronics in Amphibious Environments

Peng Du, Juan Wang, Yu-I Hsu,* and Hiroshi Uyama*

Cite This: https://doi.org/10.1021/acs.chemmater.3c02454

Read Online

ACCESS | Metrics & More | Article Recommendations | Supporting Information

ABSTRACT: Functionalized hydrogels integrating soft nature and electrical properties are of great significance for the development of human−machine interfaces, smart wearable devices, and biomimetics robotics. However, the hydrogel-based flexible sensors are inevitably utilized in aquatic environments, resulting in swelling-induced inferior mechanical performance, skin-component delamination, and monitoring malfunction. Herein, a multiple dynamic-bond-driven hydrophobic association hydrogel with reliable water resistance, mechanical robustness, and stable electrical property is proposed via a "two-step" method including micellar copolymerization and postsoaking strategy. Benefiting from the electrostatic interacted hydrophobic segments formed by myristyl methacrylate in the presence of cetyltrimethylammonium bromide micelles, the transparent hydrogel exhibits desirable antiswelling feature, excellent stretchability (∼1500% elongation), and toughness (∼2.4 MJ·m^{-3}). The synergistic mechanisms of hydrophobic association and ultrasound dispersion endow the hydrogel with repeatable wet-adhesion behaviors. Moreover, the as-prepared hydrogel possesses significant conductivity and storage durability owing to the chitosan chain entanglements, electrostatic interactions, and strong hydrogen bonding established by sodium phytate. As a demonstration, a flexible sensor is fabricated to transmit various human movement signals and wirelessly monitor electrocardiography in both air and underwater based on its wide sensing range (∼500%) and linear sensitivity. This study offers an effective strategy for developing wearable electronic systems for amphibious scenarios.

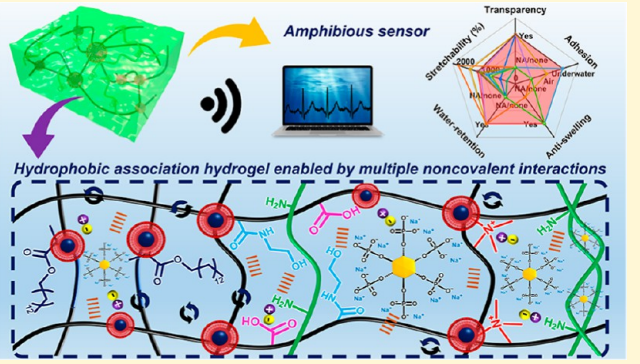

INTRODUCTION

Flexible wearable electronic devices have received growing attention across various fields, including human motion detection, healthcare monitoring, implantable bioelectronics, soft robotics, and energy harvesting.[1−5] Constructing multifunctional and dependable flexible substrates plays a crucial role in fabricating smart stretchable electronic devices. A variety of materials, such as flexible plastic, fabrics, liquid metal, and conductive elastomers, have gained considerable interest among researchers.[6−8] Among them, conductive hydrogels have become the most promising candidates for developing flexible electronics due to their biocompatibility, tunable mechanical strength, and customizable electronic performance.[9−11] Although tremendous progress has been made in conventional hydrogel sensors for terrestrial sensing, it remains challenging to avoid hydrogel swelling, maintain mechanical stability, and accurately detect electrophysiological signals by skin-worn sensors within dangerous and rigorous aquatic environments.[12−14] Therefore, multifunctional hydrophobic hydrogel electronics that can not only ensure the application in land environment but also sustain complicated water conditions are highly desired.[15−17]

So far, a great deal of effort has been devoted to designing antiswelling hydrogel materials, including increment of chemical cross-linking density, introduction of hydrophobic associations (HAs), solvent exchange, and ionic complex.[18−22] As a facile and time-saving strategy to prepare water-resistant hydrogels, HAs which can be achieved by micellar copolymerization between hydrophilic and hydrophobic monomers can assist the aggregation of hydrophobic molecules or groups with each other in water.[23,24] Then, the hydrophobic segments are connected around the micelles formed by the surfactants and become physical cross-linking points.[25] Meanwhile, the entangled network of hydrophobic chain segments significantly dissipates energy through disentanglement or sliding, thus upgrading the toughness of the hydrogels.[26] Qi et al. have demonstrated tough, robust, wet-adhesive, and antiswelling

Received: September 26, 2023
Revised: January 13, 2024
Accepted: January 16, 2024

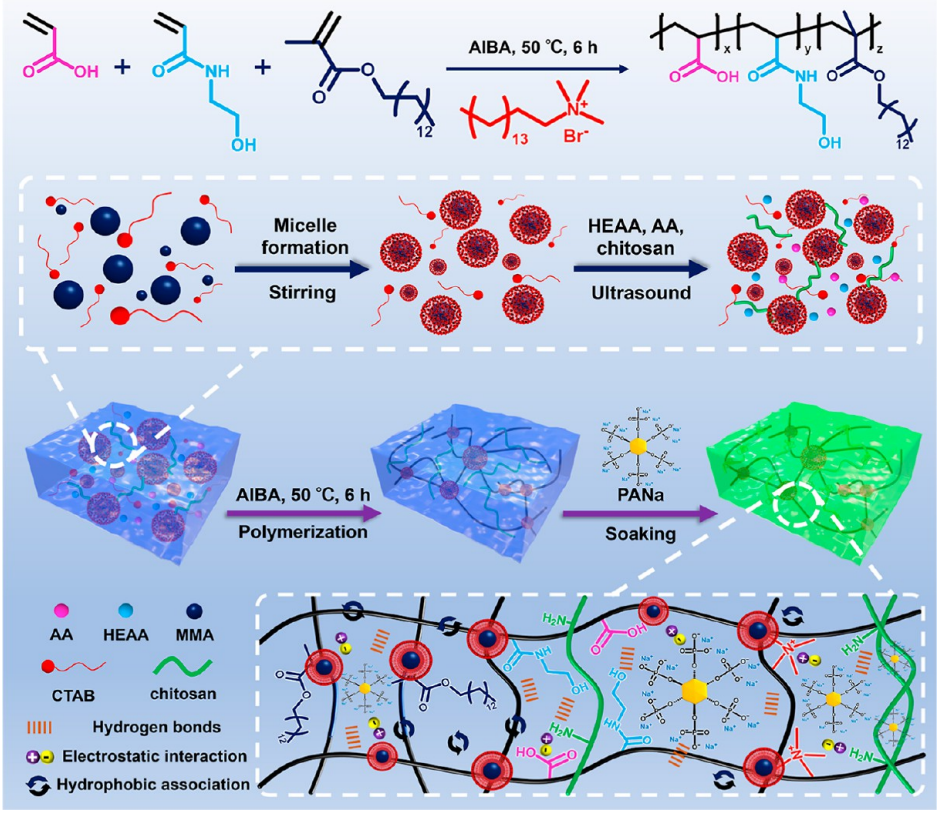

Figure 1. Mechanism illustration of constructing multiple physically interacted HA hydrogels based on a "two-step" strategy.

supramolecular hydrogels by exploiting the multiple interactions between the cationic surfactant cetyltrimethylammonium bromide (CTAB) and the copolymer of a hydrophilic monomer and hydrophobic lauryl methacrylate.[27] Tuncaboylu et al. obtained tough and self-healing hydrogels via copolymerizing hydrophilic acrylamide with hydrophobic monomer stearyl methacrylate or dococyl acrylate in sodium dodecyl sulfate and sodium chloride electrolyte.[28,29] Nevertheless, the complicated adhesion-generating processes, limited mechanical tensile strength, and weak electrical conductivity are still existing problems in hydrogels with HA alone. Therefore, developing high-performance and multifunctional HA hydrogels from eco-friendly materials using a convenient and universal method has become a trend of research.[30]

As an effective attempt, introducing synergistic electrostatic interactions into hydrophobic hydrogels can not only realize the adhesion characteristics but also improve the mechanical properties.[31,32] For instance, Huang et al. reported the hybrid hydrogels with ionically and hydrophobically cross-linked networks, where the dynamic electrostatic interactions in the hydrophobic hydrogels tuned the size of hydrophobic domains well-orderly.[33] The hydrogel was feasible to adhere to various substrates and exhibited great potential in different fields. In addition, the ionic surfactants as cross-linking points can attract oppositely charged species in the solution to form second cross-linking centers, thereby reinforcing the polymer structure with enhanced fracture toughness and stress. Demott et al. successfully combined triple network hydrogels as cartilage substitutes with synergistically intranetwork effects of HA and electrostatic repulsiveness, as well as electrostatic attractive interactions within the internetwork.[34] Despite the corresponding advantages, a flexible hydrogel strain sensor still demands to possess superior electrochemical performance, long-term stability, and transparency to function effectively.[35] Additionally, it is vital to prepare self-adhesive hydrophobic hydrogel without the complicated process of solvent replacement.[36] Rational regulation of the polymer network through a simple and universal soaking strategy will be of huge significance.[37,38]

Phytic acid (primary form of phosphorus storage in seeds and grains) was used as the gelator and dopant to form polyaniline hydrogel with record-breaking conductivity.[39] As its derivative, sodium phytate (PANa) possesses high ionization degree and abundant acceptor sites of hydrogen bonds.[40,41] Hence, it has potential that the PANa can prevent water crystallization and evaporation within the gels by hydrogen bonding with water. Chitosan, the deacetylation product of chitin, is a biopolymer extracted from shellfish such as crabs and shrimps.[42] Researchers discovered that chitosan underwent cross-linking through chain entanglement, which was initiated by shielded electrostatic repulsions between amino groups through the hydrogel soaked in a high-concentration salt solution.[43] Therefore, it is expected to stimulate the advancement of environmentally stable and multiscenario-application-capable electronic devices by immersing chitosan hydrogels into a saturated PANa solution, thereby enhancing their moisture retention, mechanical robustness, and wet-adhesion behavior.[44]

Herein, we developed a hydrogel for multiscenario application, which was composed of chitosan and electrostatic hydrophobically associated network by an efficient and simple two-step strategy. First of all, the hydrophilic monomer acrylic acid (AA) and *N*-(2-hydroxyethyl) acrylamide (HEAA) and the hydrophobic monomer myristyl methacrylate (MMA)

https://doi.org/10.1021/acs.chemmater.3c02454
Chem. Mater. XXXX, XXX, XXX−XXX

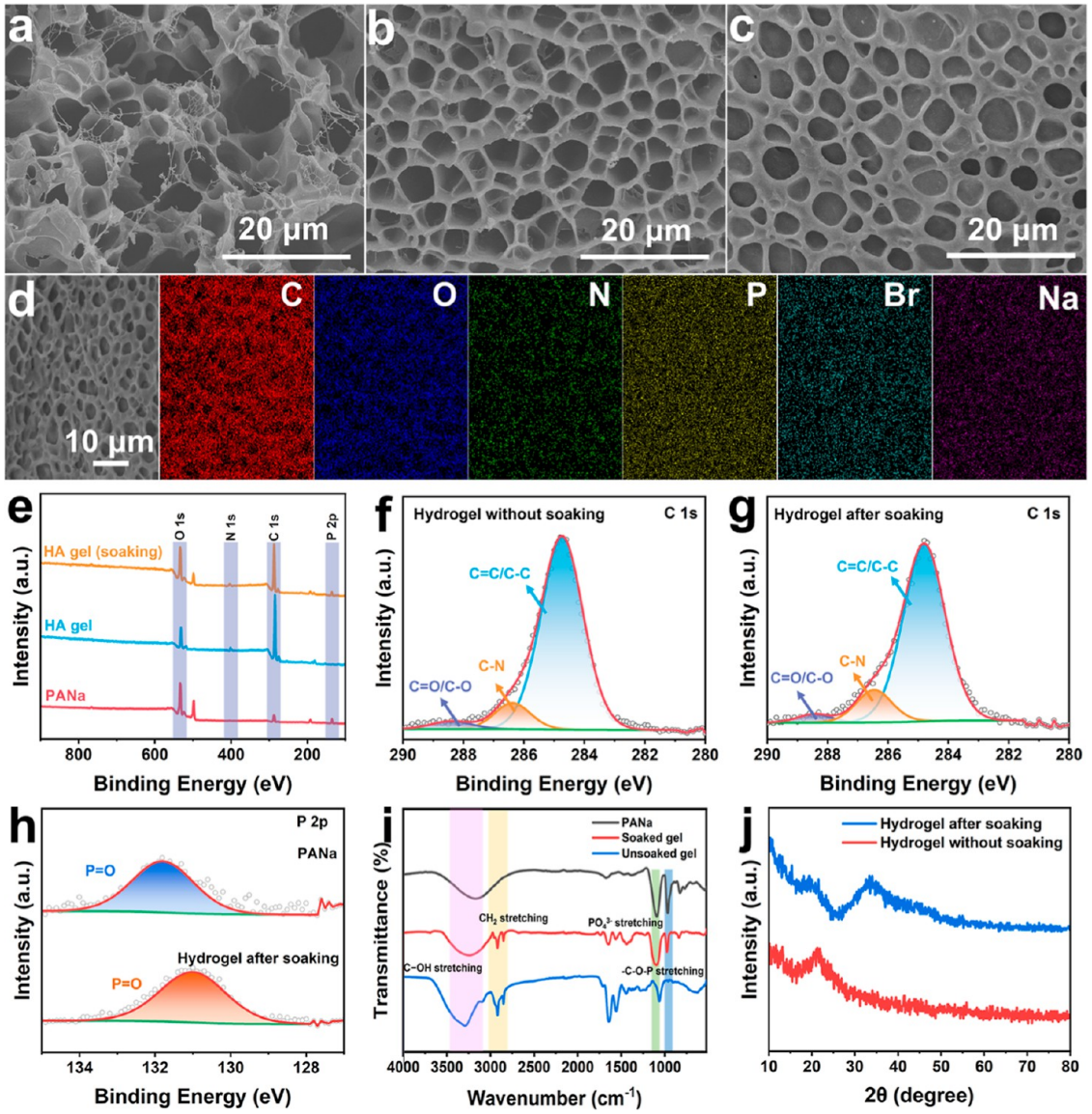

Figure 2. Cross-sectional SEM images of (a) HA hydrogel in the absence of chitosan. (b) HA hydrogel and (c) HA hydrogel after soaking in PANa solution. (d) Corresponding EDS images of soaked HA hydrogel. (e) XPS survey spectra of HA hydrogel without and after soaking and PANa. (f,g) High-resolution spectra of the corresponding hydrogels. (h) Comparison XPS spectrum of PANa and soaked hydrogel. (i) FTIR spectra of PANa, soaked hydrogel, and unsoaked hydrogel and (j) XRD patterns of the different HA hydrogels.

were randomly copolymerized with the help of the cationic micelles of CTAB after ultrasonic dispersion. On the one hand, the weak acidic environment provided by the ionization of low concentrated AA would promote the dissolution of chitosan, and the neutral HEAA monomer contains amide (−CO−NH−) and hydroxyl (−OH) groups simultaneously, which not only mimic the cement proteins of barnacles after copolymerization but also facilitate the adhesion behavior through hydrogen bonding. On the other hand, the hydrophobic segments endow the gel with certain ability to resist swelling and prevent water molecules from invading the adhesion interface. Then, the presynthesized hydrogel was soaked in statured PANa solution, resulting in (i) the chain entanglement of the chitosan backbone under shielded electrostatic repulsions and (ii) dynamic electrostatic interactions between the phosphate groups and quaternary ammonium micelles. It is worth noting that the strong hydrogen-bonding interactions between PANa and water molecules endowed the gel with a certain dehydration resistance. Overall, the multifunctional hydrogel with comprehensive performance was assembled as a sensing module to detect human motion and transmits information using Morse code in both terrestrial and aquatic environments. This work provided a new approach to designing and preparing conductive hydrogels for health-monitoring electrodes and intelligent information communicators.

RESULTS AND DISCUSSION

Design and Preparation of the HA Hydrogels. In a typical experiment, the electrostatic HA hydrogel was fabricated via a two-step strategy of random copolymerization and postsoaking method (Figure 1). Considering the balance of optimal performance, the amount of the hydrophobic monomers was 3 mol % to the total monomers, which would be discussed below, unless otherwise specified. Initially, the micelles with average size were formed through the alkyl chain

https://doi.org/10.1021/acs.chemmater.3c02454
Chem. Mater. XXXX, XXX, XXX−XXX

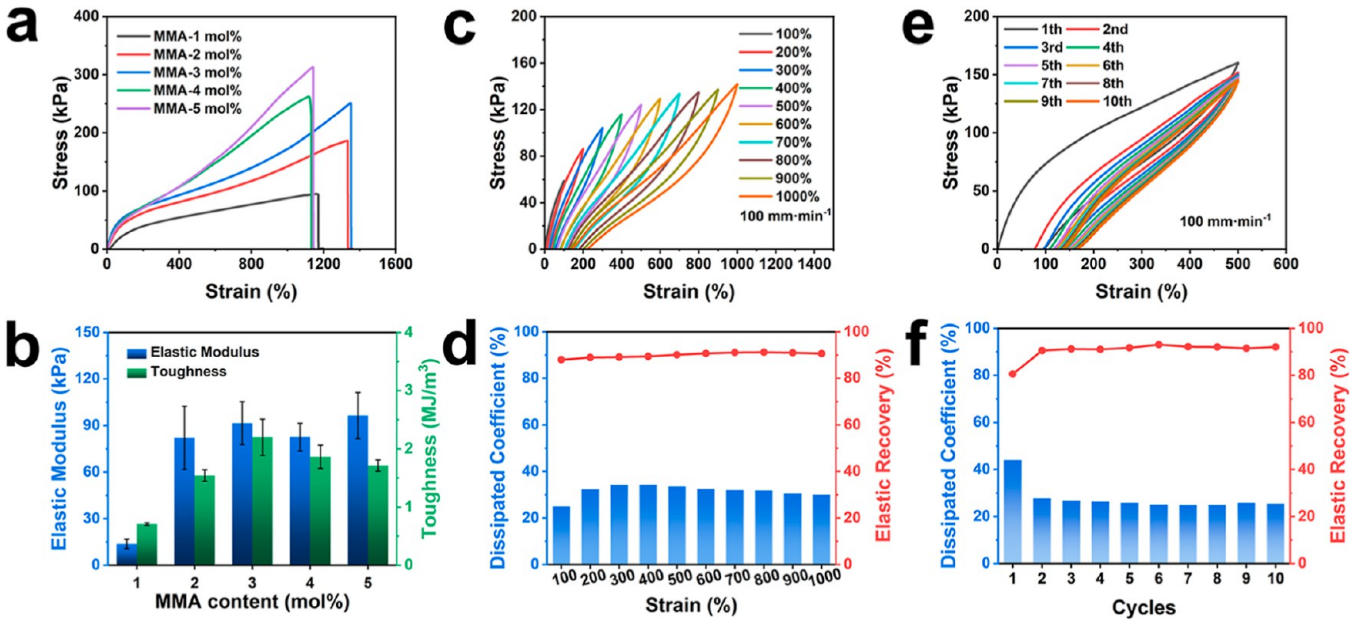

Figure 3. Mechanical properties of the HA hydrogels. (a,b) Tensile stress−strain curves of hydrogels with different additions of hydrophobic monomer MMA and the corresponding calculated elastic modulus and toughness of the hydrogels. (c,d) Successive loading−unloading curves under the strain from 100 to 1000% and the corresponding energy dissipating coefficient and elastic recovery ratio. (e,f) Cyclic curves under 500% strain for 10 cycles and the calculated energy dissipation coefficient and elastic recovery.

interactions of C_{14} unit in MMA with the cationic surfactant CTAB. After ultrasound dispersion of chitosan and precursors, the free radical polymerization including hydrophilic monomer AA, HEAA, and hydrophobic monomer MMA was carried out in a one-pot method, with CTAB as the cross-linking sites and 2,2′-azobis(2-methylpropionamide)dihydrochloride (AIBA) as the thermal initiator. Interestingly, the droplet aggregation could be avoided owing to the amphiphilic regions in chitosan.[45] The hydrophobic segments were stabilized to create a uniform hydrogel network through the chitosan, with the hydrophilic parts extending into the water, yet hydrophobic regions anchoring molecules on droplets' surfaces.[46] Subsequently, the obtained HA hydrogel was soaked in PANa solution for the second network formation.[41] In this process, the phosphate groups were permeated into the HA hydrogel because of the high osmotic gradient, then the *N*-glucosamine units within the chitosan backbone electrostatically attracted the massive negatively charged phosphate; hence, the chain-entanglement network formed because of the spontaneous collapse of chitosan chains.[47] Besides, high-density hydrogen bonds formed between chitosan chains and PANa.[48] By harnessing the synergistic effects of multiple physical interactions, the hydrogel becomes a promising candidate for mechanically robust, water-resistant, and self-adhesive strain sensors.

Structure and Characterization of the HA Hydrogels. In Figure 2a−c, the morphology of the nonchitosan-containing HA hydrogel, HA hydrogel, and soaked HA hydrogel is shown, respectively. It was apparent that three-dimensional (3D) interconnected micropores presented at the lyophilized cross-section. The scanning electron microscopy (SEM) image also revealed a great number of hydrophobic alkyl chains intertwined around the hydrophobic micelles. It evidently demonstrated that the antiswelling properties should be attributed to the massive hydrophobic cross-linking sites,[49] compared to that of the ordinary hydrogels (Figures S1 and 2). Different from the unevenly distributed porous network, the network of the HA hydrogel with chitosan in the diagram exhibited an orderly distribution. This uniform distribution of polymer chain was due to the mutual repulsion between the positively charged amino groups on chitosan backbone and the similarly charged quaternary ammonium salts in CTAB.[50] Furthermore, the "honeycomb-like" network structure indicated that the as-prepared hydrogel had an ideal surface to transfer water molecules and ions,[51] which assisted the interaction between polymer chains and the ions of PANa in the following step. As shown in Figure 2c,d, the soaked HA hydrogel had an expected morphology, and energy-dispersive X-ray spectroscopy (EDS) mapping visually proved the categories and distribution of elements in the gel. It was obvious that the hydrophobic alkyl chains stacked on the surface of the immersed HA hydrogel and demonstrated a wrinkled structure. The phenomenon could be attributed to the increased cross-link density caused by strong hydrogen bonding and chain entanglement.[52] As a result, the synergies of physical interactions and interconnected conductive paths were potentially beneficial for the mechanical properties and electronic performance of the hydrogel.

To examine the key element presence and hydrogen bonding interaction in the gel, X-ray photoelectron spectroscopy (XPS) was conducted. As illustrated in Figure 2e, the elements of O, N, C, and P were confirmed, which were consistent with the raw materials used. Next, more specific XPS analysis of the high-resolution spectrum can determine the effect of the soaking process on the hydrogel. The high-resolution spectrum of C 1s orbit for both HA hydrogels could be deconvoluted into three characteristic peaks: the C═C/C−C (284.8 eV), C−N (286.3 eV), and C═O/C−O bond (289 eV) (Figure 2f,g).[53] Compared with the results in PANa (Figure S3), the emerging C−N component peak confirmed the presence of nitrogen elements. Meanwhile, the N 1s characteristic peaks in Figure S4 were ascribed to N−C═O

https://doi.org/10.1021/acs.chemmater.3c02454
Chem. Mater. XXXX, XXX, XXX−XXX

and N−C, respectively,[54] further indicating the existence of hydrophobic segments and chitosan. In Figure 2h, the comparison XPS spectra between PANa and soaked gel was evidence to confirm the hydrogen bonding interaction. The characteristic peaks at 132 and 133 eV were assigned to the P═O groups of PANa and PANa-soaked hydrogel, respectively.[41] The decreased binding energy indicated the formation of hydrogen bonds in hydrogel, where the PANa could serve as a salt to intensify the conversion of polymer aggregation.[55]

Attenuated total reflectance−Fourier-transform infrared (ATR−FTIR) spectroscopy was employed to further analyze the chemical structure and interaction of the HA-hydrogel-related materials (Figure 2i). PANa exhibited typical stretching vibrations of the HPO_4^{2-}, PO_4^{3-}, and C−O−P groups around 1656, 1090, and 992 cm^{-1}, respectively.[41,53] Although there was a red shift in both PO_4^{3-} and C−O−P stretching vibrations in the PANa immersed hydrogel, the broadened peak could be attributed to the influence of hydrogen bonds that impaired the original bond energy.[56] The same phenomenon occurred in the comparison spectrum of the HA hydrogels. Specifically, the characteristic peaks at 3286 and 2896 cm^{-1} corresponding to C−OH stretching and CH_2 stretching in hydrogel without soaking shifted to lower wavenumber of 3256 and 2880 cm^{-1}, respectively. The weakened chemical driving force led to declined vibration frequency of the chemical bonds.[57] Therefore, it further confirmed the formation of hydrogen bonding in the chitosan network and gel polymer backbone. The aggregated structures of HA hydrogels with chitosan addition could be characterized by X-ray diffraction (XRD) patterns (Figure 2j). The XRD pattern of the HA hydrogel without soaking showed low-intensity characteristic peaks at around 20°, which superimposed crystallization diffraction of the (220)/(200) crystal plane for chitosan crystal hydrates.[58] However, the salting out effect led to a decrease of crystal plane spacing and crystallinity, as evidenced in Figures 2j and S6, demonstrating the influence of PANa on the aggregated structure of chitosan in both pristine and dehydrated hydrogels.

Mechanical and Viscoelastic Properties. The presence of a hydrophobic monomer and chitosan is crucial to affect the mechanical properties, which even determines the sensing reliability of the conductive hydrogel. Therefore, the mechanical properties reflecting the influence of MMA (from 1 to 5 mol %) were systematically investigated by the universal tensile test (Figure 3). From the typical stress−strain curves, the HA hydrogels showed an improved tensile strength, while the tensile strain decreased with the increase of MMA concentration from 3 to 5 mol %. However, the hydrogels with hydrophobic MMA below 3 mol % exhibited poor mechanical properties with a fracture stress of lower than 200 kPa (Figure S8), and both the tensile stress and tensile strain were positively correlated with MMA concentration in the range of 0−2 mol %, indicating that the massive cationic surfactant had an impact on the mechanical properties before sufficient hydrophobic cross-linking segments formed. When the MMA was increased to 3 mol %, the HA hydrogel formed enough cross-linked structures, thereby improving the tensile properties. Although the hydrogel with 4−5 mol % MMA exhibited high strength, both had impaired stretchability of less than 1200% due to the inhomogeneous distribution of redundant MMA segments.[59] The results are in accordance with the cross-sectional SEM diagrams in Figure S5. Based on the results, we believe that the HA hydrogel could obtain optimal mechanical performance with a fracture stress of 255 kPa and a stretchability of 1360%. Furthermore, the calculated elastic modulus and toughness in Figure 3b are another piece of evidence to prove the superior elasticity and strength, and the MMA-3 mol % HA hydrogel reached the highest toughness of 2.28 $MJ·m^{-3}$ and Young's modulus exceeding 90 kPa. As a comparison, the effect of adding chitosan is discussed in Figure S8. The tensile strength of the pure hydrogel without chitosan was too low to be practically applied, and it exhibited a semifluid-like consistency due to its weak cohesion.[60] Despite the addition of chitosan, the lack of a hydrophobic domain and only weak physical cross-linking led to insufficient elasticity and strength. Amazingly, under the synergistic effect including the hydrophobic domain and chitosan cohesion, the breaking stress ended up being five times that of the pristine hydrogel, which was consistent with the compression tests (Figure S9).

To further prove the elasticity and restoration of the MMA-3 mol % HA hydrogel, loading−unloading test was conducted. The curves in Figures 3c,d and S10a showed the typical cycling test under different strains ranging from 100 to 1000% and their corresponding results of dissipated coefficient and elastic recovery. It could be observed that the HA gels at different strains exhibited increasing hysteresis loops, indicating an effective energy dissipation.[61] As the strain increased, the hydrogel dissipated more energy while achieving a stable energy dissipation ratio around 30% and elastic recovery of 90%. This phenomenon could be explained by the synergistic effects of various physical interactions.[62] For example, the hydrophobic segments detached at small strains, breaking into small clusters for effective energy dissipation, but reconstructed into a network accompanied by chitosan through the reversible nature of hydrogen bonds.[63] Moreover, the stress−strain curves of the hydrogel exhibited distinct hysteresis loops at a fixed strain of 500% (Figure 3e). As far as known, the inner polymer network of hydrogel was easily weakened to a large extent and thereby cannot be instantly restored after the first loading. However, after the following nine stretching cycles, there were no apparent shape and stress loss, so that the hydrogel could partly recover because of the reconstruction of multiple physical interactions.[64] The dissipated energy and resilience were analyzed, as shown in Figures 3f and S10b. The quantified energy dissipation was stabilized around 80−100 $kJ·m^{-3}$ except for the first cycle, and the value of elastic recovery maintained at 90%, which demonstrated high elasticity and self-adaptability to successive stretching. This was mainly due to the multistage physical interactions and hydrophobic domains.[47]

However, the single effective HA hydrogel was unable to form the secondary chitosan network structure and dynamic electrostatic interactions. Consequently, the mechanical strength, swelling resistance, adhesive behavior, and electronic performance failed in meeting the requirements of a flexible sensor. Soaking in PANa solution as a facile and effective strategy was adopted in the following research. As shown in Figure S11, the tensile behaviors of the hydrogels soaked for different time and in different solution concentrations were compared. The tensile strength and strain increased to 430 kPa and 1500%, respectively, with the increasing PANa solution concentration, indicating that the hydrogels could absorb large amounts of ions under high osmotic pressure. Moreover, immersing the hydrogel in a saturated solution for 45 min was sufficient to endow it with optimal stiffness and toughness. The strong electrostatic interaction promoted chain entanglement

https://doi.org/10.1021/acs.chemmater.3c02454
Chem. Mater. XXXX, XXX, XXX−XXX

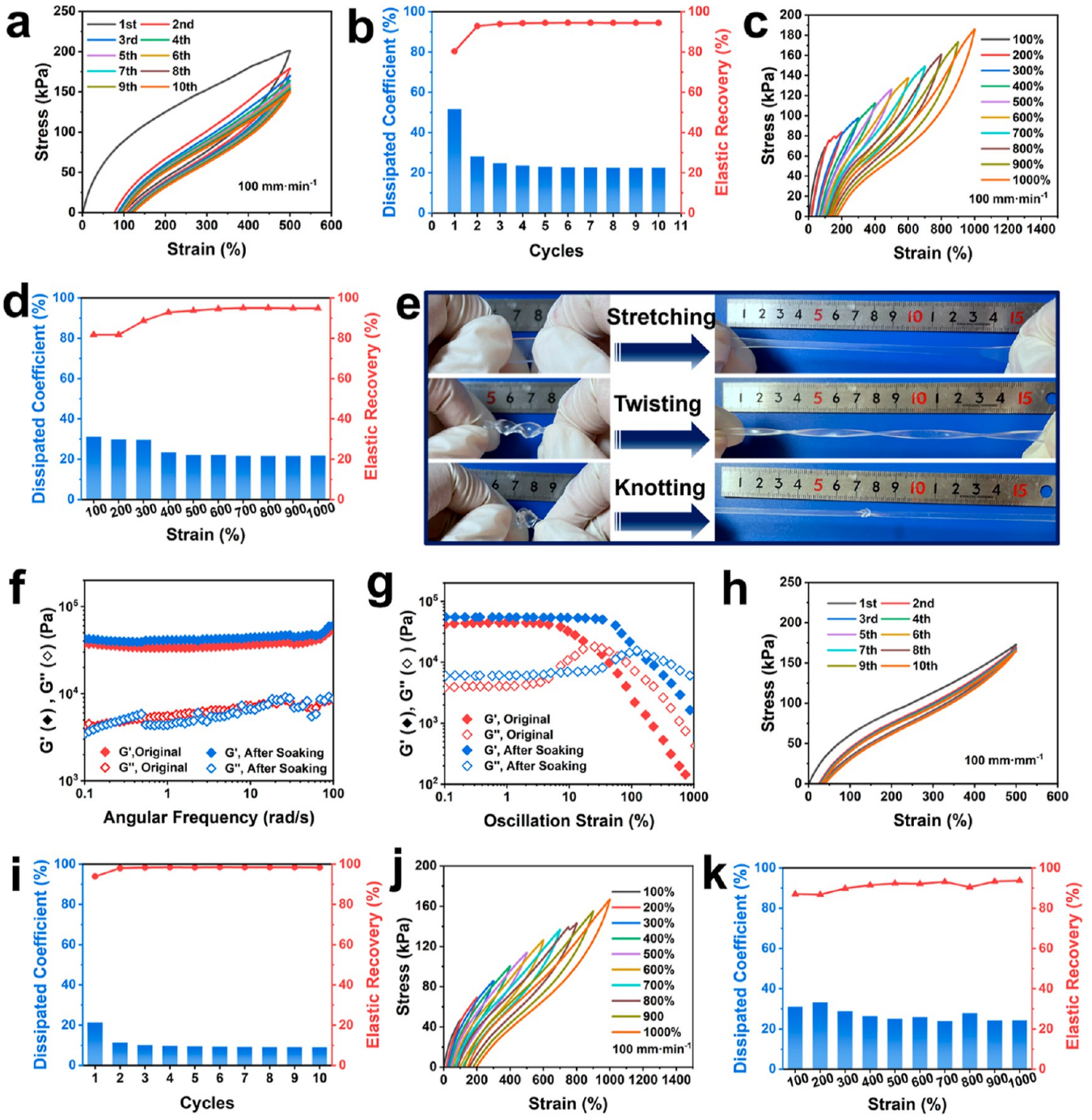

Figure 4. Mechanical properties of the hydrogels in air. (a) Cyclic strain test under 500% stretching for 10 cycles. (b) Corresponding energy dissipation and elastic recovery. (c,d) Successive tensile loading−unloading curves of the electrostatically interacting HA hydrogel at different strain and their corresponding energy dissipation coefficient and elastic recovery. (e) Optical images of manual stretching of hydrogels in different deformation forms; rheology analysis of the gel. (f,g) Rheological behavior at varying angular frequencies and the dynamic shear scanning. Mechanical properties of the electrostatic interacted HA hydrogels underwater. (h,i) Consecutive loading−unloading stress curve at a strain of 500% (10 cycles) and the calculated hysteresis ratio and elastic recovery; (j,k) loading−unloading strain curves ranging from 100 to 1000% and the corresponding dissipating coefficient and elastic recovery.

of chitosan that comprised the strong interpenetration with hydrophobic domains and enhanced the mechanical strength.[43]

Correspondingly, the excellent hysteresis and shape-recovery behavior induced by the multistage dynamic bonds were investigated, as shown in Figure 4a−e. The ten successive cyclic tensile loading−unloading curves displayed a noticeable hysteresis loop with residual strain, indicating a significant capacity for energy dissipation. The larger hysteresis area of the first cycle reflected the dissociation of entanglement and hydrogen bonds broken, and the following nine cycles showed a significant recovery of dynamic bonds.[47,64] In contrast, the elastic recovery ratio and dissipated coefficient became 95 and 22%, respectively, in following cycles, which indicated that the postimmersing hydrogel was incorporated with massive electrostatic interactions to reverse the self-recovery ability

https://doi.org/10.1021/acs.chemmater.3c02454
Chem. Mater. XXXX, XXX, XXX−XXX

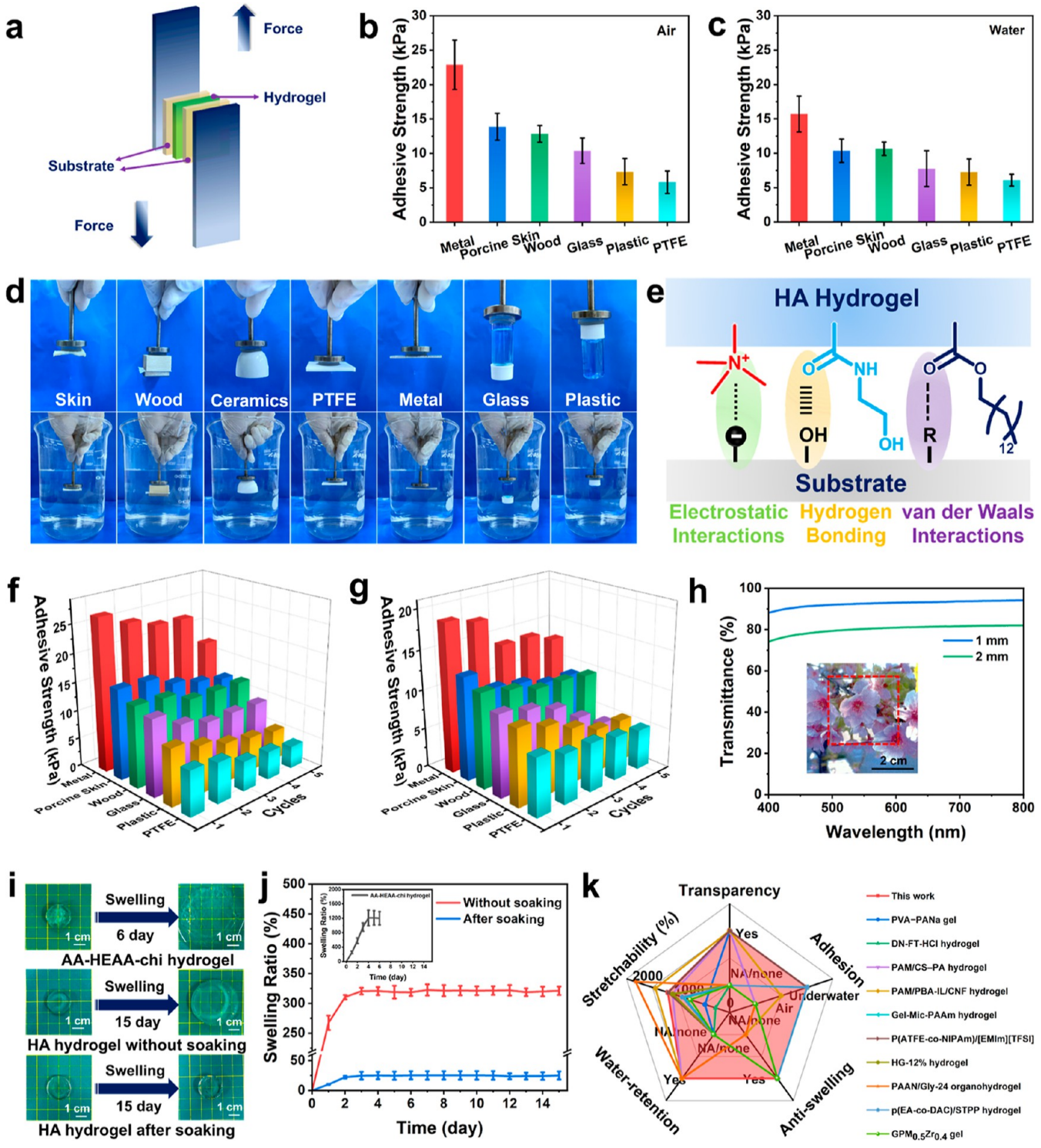

Figure 5. Adhesion behavior of the hydrogel. (a) Schematic of the lap shear test. (b,c) Lap-shear adhesion strength of the hydrogels on diverse substrates in air and underwater, respectively. (d) Photographs of the hydrogel adhering to different substrates in air and underwater. (e) Illustration of the adhesion mechanism. (f,g) Repeatable adhesive strength curves of the hydrogels to various substrates conducted by five successive attaching−detaching processes (in air and underwater). (h) Optical transparency of the electrostatic interacted HA hydrogel; swelling behaviors of the hydrogels with different ingredients. (i,j) Optical pictures and swelling ratio curves; (k) chart comparison between the hydrogel used in this work and previous reported gels in the aspects of transparency, adhesiveness, antiswelling, dehydration tolerance, and stretchability.[30,33,36,40,41,66,67,69−71]

rapidly. The hysteresis loop in cyclic loading−unloading tests at different strains from 100 to 1000% was positively correlated with the tensile strain in Figures 4c and S13. More dynamic bonding after soaking played an important role in efficiently consuming the internal network energy when subjected to external stress. Therefore, the electrostatically interacting HA hydrogel showed high elasticity and self-adaptability to cyclic stretching within a wide strain range of 400−1000%. As

https://doi.org/10.1021/acs.chemmater.3c02454
Chem. Mater. XXXX, XXX, XXX−XXX

intuitive evidence, the optical pictures in Figure 4e demonstrated that the soaked HA hydrogel possessed significant robustness and toughness. It could be not only directly stretched to 15 times its original length but also easily stretched in twisting and knotting states.

The viscoelastic behavior of the electrostatic HA hydrogels without and after soaking was assessed by oscillatory rheology measurements at 25 °C. Figure 4f shows the frequency dependence of storage modulus (G') and the loss modulus (G''). Both values increased with the increase of the angular frequency, whereas G' was consistently greater than G'', indicating the typical elastic solid-like behavior of hydrogel. The value of G' after postsoaking was consistently higher than that without immersing, which demonstrated an enhanced elasticity and could be attributed to the abundant dynamic effects of HA interactions and hydrogen bonds. Besides, there was no significant change for G' and G'' when subjected to low-range strain in Figure 4g. The G' value of the unsoaked gel dramatically decreased at 8% strain and intersected G'' at 11% strain. However, in a soaked hydrogel, the G' sharply decreased at 30%, illustrating that the enormous dissipating energy made it more resistant to collapse.[65] And, the significantly improved intersection strain of 150% also proved that electrostatic interactions enhanced the hydrophobic domain to resist deformation effectively.

For underwater application, it was necessary for the hydrogel to show a mechanical response to external strain in aquatic condition. The hydrogel was fixed on a water container with the universal strain tester. It was observed that the calculated elastic modulus and toughness showed no apparent change whether in air or water (Figure S14). Moreover, the dissipative energy capability of the as-soaked HA hydrogel underwater was examined by cyclic loading−unloading tests (Figure 4h−k). The hydrogel exhibited a negligible hysteresis loop in deionized water after ten successive cycles stretches under 500% strain. The hysteresis ratio was kept at 8% with an energy dissipation of ∼43 kJ·m^{-3} and showed an excellent resilience of 95% elastic recovery. As seen from Figure 4j, expanding hysteresis loops appeared when applying the hydrogel to different strain from 100 to 1000%. But the material showed a stable energy dissipating coefficient (30%) and elastic recovery (95%), indicating an excellent mechanical performance underwater application. Although the overall trend is consistent, we speculated that the low hysteresis underwater could be attributed to inhibitory formation of extensive hydrophobic domains.[31] Since the hydrogen bonding with water enhanced the polymer−water interaction force, the equilibrium with elastic retractive force induced by electrostatic interactions between PANa and HA segments was influenced, resulting in weakened mechanical performance underwater.[66] The results were consistent with interval rest cyclic tensile experiments; thereby, the hydrogel displayed favorable endurance and compliance in multiple environments.

Adhesive Performance and Underwater Stability. In addition to excellent mechanical properties, hydrogels exploited as wearable sensors need to achieve functional characteristics. The hydrogel could directly adhere to diverse substrate materials including paper, stone, porcine skin, metal, rubber, and ceramics without extra auxiliary binders (Figure S17). Therefore, a lap shear test was employed to quantify the self-adhesion capability. In Figure 5b,e, the hydrogel showed the highest adhesion strength to metal surface due to the synergistic effect of van der Waals force and hydrogen bonding generated between hydrogel and the metallic surface.[67] Moreover, the electrostatic interactions and strong hydrogen bonds were the two main effects responsible for the adhesion toward ceramics, plastic, polytetrafluoroethylene (PTFE), glass, rubber, porcine skin, etc. Besides, the effective adhesion based on reversible physical interactions exhibits reproducibility and durability (Figure 5f). After cyclic shear experiments, although the adhesion strength decreased slightly in cyclic shear experiments, it still maintained over 67% of the initial value after five peelings. Therefore, the reversible physical interaction endowed the gel with good compatibility and reproducible adhesion, enabling the materials to chronically adhere to various substrates without external assistance. It showed great application potential without compromising the mechanical properties in wearable strain sensors.

The adhesive behavior of the soaked hydrogel underwater to diverse substrates was also investigated (Figure 5a). The hydrophobic interface could disrupt the hydration layer formed on the hydrogel surface, facilitating the establishment of a robust connection between the target interfaces. Therefore, after 30 s compression, the hydrogel showed stable adhesion to various substrates in both air and underwater (Figure 5d). The average adhesive strength by underwater lap shear test of the hydrogel to metal, skin, wood, glass, plastic, and PTFE were 19, 13, 12, 10, 9, and 7 kPa, respectively (Figure S19, Movie S1). Although the wet adhesion forces were slightly reduced during five successive experiments (Figure 5g), the hydrogel still demonstrated effective robust and long-term underwater adhesion for practical application. The hydrophobic micelles, electrostatic interactions, and ultrasonic recombination not only offered several adhesive mechanisms but also prevented the water molecules invading the contacting interfaces (Figure 5e).[68]

Generally, the hydrophobic hydrogels were prone to become opaque due to the formation of the heterogeneous hydrophobic domain in water. It was necessary to explore the transparency of hydrogels, which is accompanied by underwater adhesion. As shown in Figure 5h, the hydrogel was highly transparent at room temperature because the inset pattern covered by a hydrogel could be clearly observed. The UV−vis transmittance for hydrogels with thicknesses of 1 and 2 mm reached over 90 and 80%, respectively, at a wavelength of 550 nm, which was enough for visualization of wearable sensors.

The above-mentioned applications involved underwater stability, so the antiswelling properties of hydrogels were discussed. The hydrogel AA-HEAA-chi without hydrophobic segments easily dissociated and had difficulty in maintaining integrity (Figure 5i,j). Ultrasonic dispersion avoided the violent aggregation of hydrophobic micelles; the electrostatic interaction promoted the formation of well-ordered hydrophobic domains in gel network. In this case, the hydrogel exhibited great potential in water-resistance performance. The unsoaked HA hydrogel showed a distinct rise in diameter after 15 d immersion in deionized water compared with that in PANa-soaked hydrogel. The phenomenon demonstrated that hydrophilic−hydrophobic copolymers could locally adsorb water due to the heterogeneous hydrophobic structures, while the electrostatic-interaction-induced dynamic HA could tune hydrophobic domains effectively to inhibit water penetration.[20] The swelling capability of electrostatically interacting HA hydrogel was maintained at 25% and evidenced the well-behaved water resistance compared with that of the ordinary

https://doi.org/10.1021/acs.chemmater.3c02454
Chem. Mater. XXXX, XXX, XXX−XXX

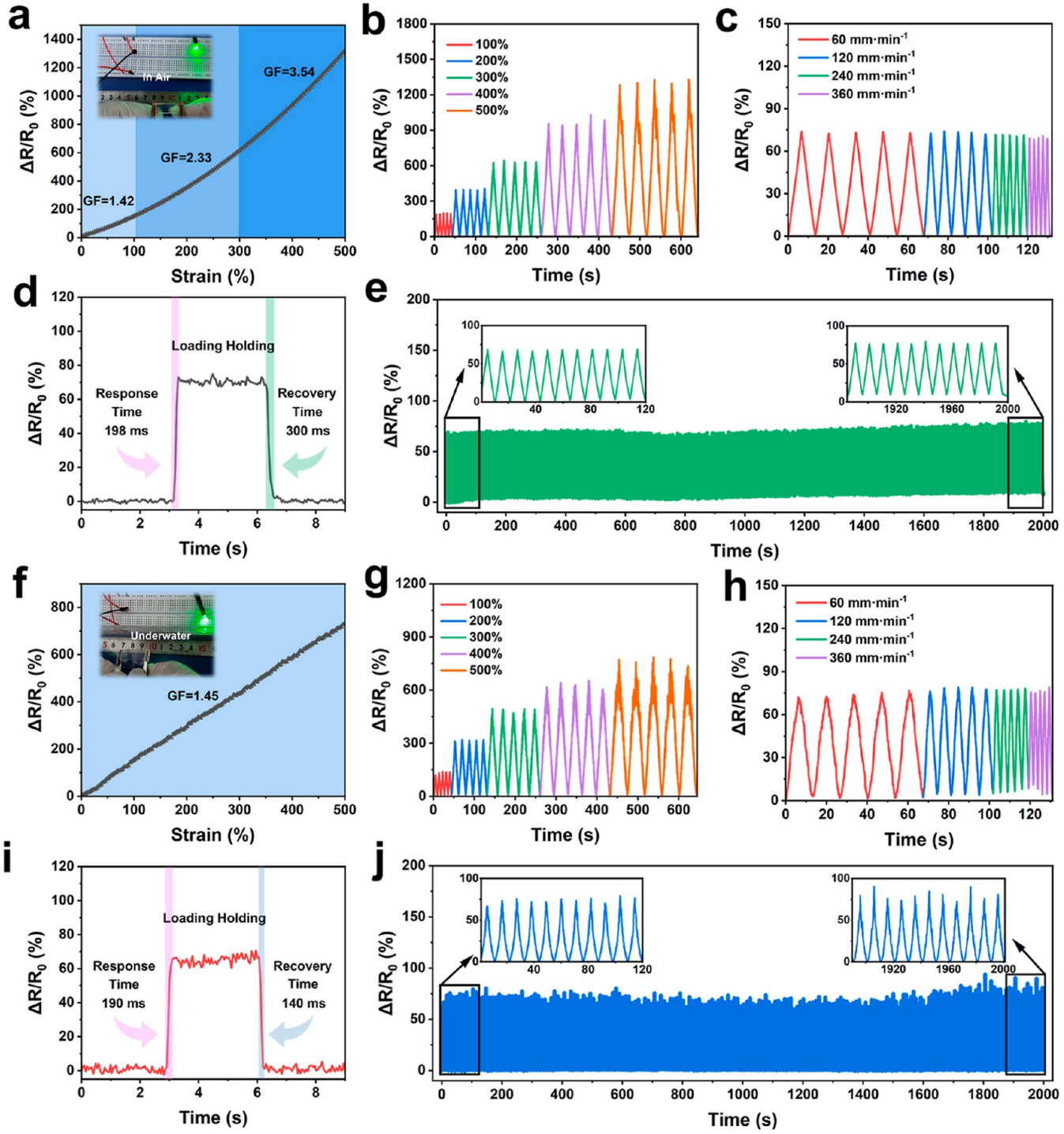

Figure 6. Electrical sensing performances of the hydrogel strain sensor in air. (a) Relative resistance changes with strain in the range of 0−500%. (b,c) Relative resistance changes under representative strain and frequencies; (d) response and recovery time curve of the hydrogel sensor. (e) Repetitive resistance changes upon cyclic stability test at a fixed strain of 50%. Sensing performances of the hydrogel strain sensor underwater. (f) Relative resistance changes as a function of the applied strain. Resistance changes of hydrogels upon cyclic loading−unloading measurement within (g) various strains, and (h) different tensile speeds. (i) Response and recovery time of the sensor underwater. (j) Electromechanical stability of 200 cycles under 50% strain.

hydrophobic hydrogel with a swelling ratio of 320%. Moreover, water contact angle (WCA) was employed to characterize the surface hydrophobization property of the hydrogels (Figure S21). With the increasing concentration of MMA, the WCAs of the HA hydrogel increased from 78.1 to 110.7°, indicating enhanced hydrophobicity on the gel surface because of a significant number of surfactant alkyl chains and C_{14} units. Notably, PANa had little effect on the hydrophobic nature, so that the HA hydrogel after soaking treatment still exhibited significant hydrophobicity. In addition to the hydrophobic capability, this hydrogel-based sensor displayed antidehydration feature that was a prerequisite for applications under extreme conditions. The HA hydrogel demonstrated a certain level of water retention of 64% after 15 days of storage (Figure

https://doi.org/10.1021/acs.chemmater.3c02454
Chem. Mater. XXXX, XXX, XXX−XXX

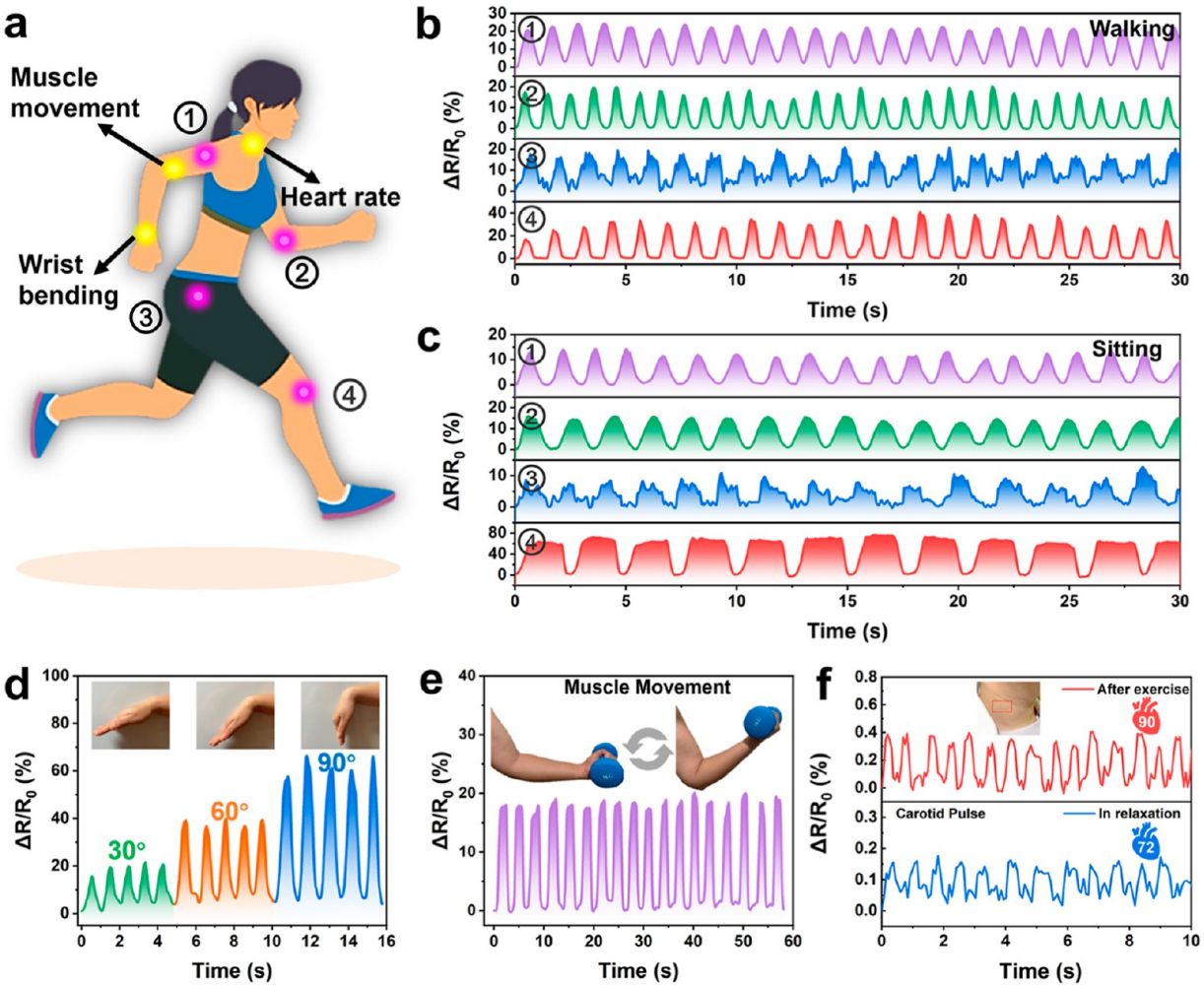

Figure 7. Human motion sensing in real time by the hydrogel sensor. (a) Description of the detection locations in a body. Sensing signals of relative resistance variations on multiple sites of shoulder, elbow, hip, and knee during (b) walking and (c) sitting. Real-time relative resistance of (d) wrist movements in different angles and (e) muscle movement. (f) Carotid pulse measured through a time-dependent relative resistance change.

S22). Surprisingly, the residual weight ratio of the post-immersed hydrogel remained at 84% which showed a better moisture retention performance owing to the even dispersion of the C_{14} alkyl group on the gel surface. As depicted in Figure 5k, this hydrogel combined adhesion, transparency, water-retention, antiswelling, and stretchability. It was undoubtedly a crucial candidate for developing intelligent wearable devices both in air and underwater.

Electromechanical Properties. PANa is a strong electrolyte that releases large amounts of sodium ions (Na^+) through ionization. The Na^+ in the porous microstructure, as well as the bromide ions (Br^-) from CTAB, granted the hydrogel with a conductivity of 2.9 mS·cm^{-1} (Figure S24). To prove the feasibility, a light-emitting diode (LED) was connected into a 3 V-powered circuit, where the hydrogel was applied as a variable resistance. When the hydrogel was subjected to repeated stretches, the darkness of the LED changed with the length of the hydrogel (Movie S2). Consistent with the law of resistance, the ion transmission in the stretched hydrogel became difficult when the conduction path got narrower and longer, resulting in an increasing resistance. Because of the reliable mechanical performance both in air and underwater, the varying resistance of hydrogel contributed to the LED luminance change.

Similarly, the strain sensitivity in a wide range was investigated in air and water. In air, the gauge factor (GF), calculated by the ratio of relative resistance change ($\Delta R/R_0$) to strain (ε), was divided into three regions (Figure 6a). Specifically, the GF values were 1.42, 2.33, and 3.54 in the strain range of 0−110%, 110−300%, and 300−500%, respectively, and each complied with a high linearity with the applied strain. The trait of hydrogel acting like a human epidermis was derived from the excellent strain sensitivity on the basis of ionic conductivity and mechanical properties. As shown in Figures 6b and S25, the resistance change ratio demonstrated the repeatability and strain dependency from 2 to 500% strains at the five stretching−releasing cycles. Besides, at a fixed strain of 50%, the hydrogel could distinguish the varying frequencies and exhibited unanimous relative resistance peaks (Figure 6c). Therefore, it was obvious that the hydrogel system possessed superior signal stability and repeatability. Notably, a significantly fast response time (198 ms) and recovery time (300 ms) were detected to evaluate the signal response speed (Figure 6d). The responding rates were sufficient to meet the requirements of real-time human motion monitoring. Most importantly, the hydrogel sensor suffered minor signal attenuation and drift upon consecutive cycles for

https://doi.org/10.1021/acs.chemmater.3c02454
Chem. Mater. XXXX, XXX, XXX−XXX

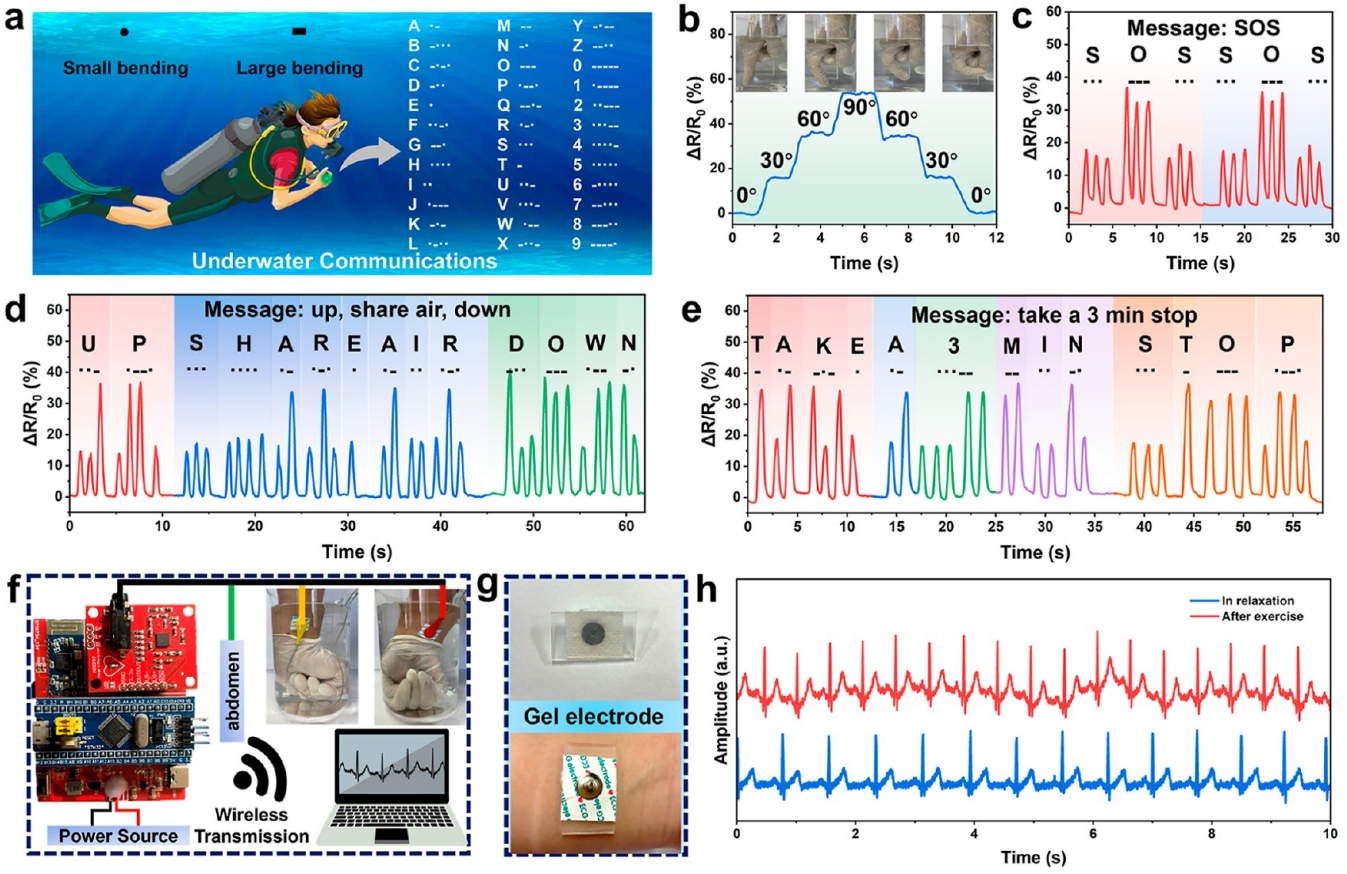

Figure 8. Applications for underwater physiological monitoring. (a) Schematic design of the underwater communicator based on Morse code. (b) Electrical response under different amplitudes through the finger bending in water. Practical underwater applications of recoding raw signals of (c) "SOS", (d) "up", "share air", and "down", (e) "take a 3 min stop". Wearable bioelectronics in an aquatic environment. (f) Diagrams of wireless ECG monitoring. (g) Assembled hydrogel electrode. (h) ECG signals captured by the hydrogel sensor.

200 times at 50% strain, indicating the satisfying durability (Figure 6e).

Alternatively, corresponding electromechanical measurements underwater were carried out, as illustrated in Figure S23. The adhesive ability and underwater stability ensured that the antiswelling hydrogel was fabricated as an underwater strain sensor. As shown in Figure 6f, the GF reflecting underwater was calculated, where the relative resistance increased linearly upward with strain. The GF value reached 1.45 in the strain range of 0−500%, which was superior performance compared with that of the reported parameters underwater.[17] The decreased GF in water was attributed to the conductive pathway in a homogeneously ordered hydrophobic structure facilitating ion transmission, yet fewer freely moving ions reduced the sensitivity. This phenomenon was also confirmed by the underwater sensing when applied with different strains and frequencies (Figure 6g,h). It was observed that the hydrogel showed good responsiveness to the stretching−relaxation process, proving that it had excellent underwater sensitivity to different strain amplitudes. Even if the stretching speed changed, the resistance change ratio remained basically unchanged, indicating that the hydrogel had favorable sensing stability. Moreover, in Figure 6i, the underwater strain sensor displayed faster response and recovery times of 190 and 140 ms, respectively, demonstrating a perception speed close to human skin.[23] To prove the long-term electromechanical stability, 200 cycles of continuous stretching at 50% strain were conducted. As shown in Figure 6j, the relative resistance change was maintained almost the same in the whole repeated period. Owing to the well-ordered hydrophobic structure, the ions could transfer freely in a water environment. Overall, the high flexibility, strain-sensing stability, and durability ensured the prominent reliability of the underwater sensor.

Real-Life Demonstration as Human Activity Monitoring Sensor. To take advantage of the excellent sensing performance and superior mechanical properties, the hydrogel was applied as a strain sensor to detect human physiological motions in real time. As shown in Figure 7a, the hydrogel was directly attached to different parts of a human body, and resistance signal was recorded synchronously. To evaluate the feasibility of the hydrogel sensor in human activity detection, the main joints including shoulder joint, elbow joint, hip joint, and knee joint of the human body were taken as the monitoring points to verify the body postures while simulating walking and sitting. The output data in Figure 7b,c confirmed the possibility of distinguishing different body postures according to discrepant frequencies of the resistance change and waveforms of the signals. Furthermore, to prove the stability of the wearable device, electronic signals based on the bending movement of the wrist were recorded through multiple bending−releasing cycles at different angles (Figure 7d). The resistance signal changed and then restored to its original value when the wrist was bent and straightened, demonstrating high repeatability and stability at wrist bending angles of 30, 60, and 90°.

https://doi.org/10.1021/acs.chemmater.3c02454
Chem. Mater. XXXX, XXX, XXX−XXX

The stable and accurate signal detection of the hydrogel sensor ensures its suitability for applications in health management. In actual movement scenarios, it aided in life-quality improvement and disease prevention by analyzing signals such as muscle movement and heart rate in real time. Thus, the resistance was examined in both large deformations and subtle movements, (Figure 7e,f). Based on the adhesion behavior and stretchability, the sensor exhibited a specific waveform of muscle movement by lifting dumbbells even if the skin was sweaty. Moreover, the hydrogel device was attached to the neck to track the carotid rates because of its sensitivity. The carotid pulse rate was 72 beats min^{-1} under relaxing circumstances but increased to 90 beats min^{-1} after exercise. This hydrogel sensor with adhesiveness and antiswelling ability demonstrated reliable sensitivity and stability even when skin tended to become moist after exercise.

Underwater Physiological Signal Detection and Communication. As continuous exploitation for marine resources, underwater communication has garnered significant attention for its capacity to convey information in real time and enhance the safety conditions of diving operators. Given the impressive combination of mechanical performances, antiswelling abilities, adhesive behaviors, and electrical sensitivity of the hydrophobic hydrogel, it ensured the practical underwater sensing application. Morse codes were utilized to convey information for divers wearing the gel sensor. Here, the "dots" and "dashes" in coding principle were matched with the finger bending states (Figure 8a). Based on the step signals corresponding to finger bending angles in Figure 8b, it was determined that 30° (small) bending gesture and 60° (large) bending angle would represent "dots" and "dashes" in this information transmission mechanism underwater. As a validation, several demonstrations of the relative resistance change in different underwater scenarios were carried out. In Figure 8c, the divers could send distress message of "SOS" by rhythmically bending fingers to request assistance when they encountered emergency situations. More meaningfully, during deep-water operations such as exploration, salvage, and rescue, the underwater communicator enabled the subaquatic operators to request ascending, descending, and oxygen supplement from the terrestrial personnel by sending a sequence of phrases (Figure 8d). The hydrogel sensor could also convey information in complex (sentences) form. As shown in Figure 8e, the diver could avoid the "decompression sickness" symptom after operation via reminding their partners to follow slow ascent guidelines by sending a lengthy message of "take a 3 min stop". Therefore, the hydrogel sensor offered a viable means of underwater information transmission.

To further investigate the application of the hydrogel in an aquatic environment, the wet-adhesive hydrogel was fabricated into a wireless electrocardiogram (ECG) device as a flexible electrode (Figure 8f,g). During heartbeats, the depolarization of myocardial cells causes a minor electrical signal on the skin surface, which was received by the hydrogel electrode.[72] The analog signal was collected by filtering and amplification processing in the AD8232 module and then captured by the STM32 analog to digital converter. Due to the significant antiswelling and self-adhesive properties, the hydrogel-based bioelectronic coating exhibited stable ECG measurement compared with that by a commercial electrode (Figure S26). Hence, the hydrogel electrode demonstrated promising application in underwater ECG detection and wireless transmission in the relaxing state and after exercise (Figure 8h). As demonstrated above, the hydrophobic hydrogel sensor showed great potential in constructing wearable bioelectronics in an aquatic environment.

CONCLUSIONS

In summary, a novel electrostatically interacting HA hydrogel with underwater adhesiveness was successfully developed by a facile "two-step" method. In this strategy, random polymerization between hydrophilic monomers HEAA and AA and hydrophobic monomers of MMA was cross-linked in the presence of cationic surfactant micelles CTAB, followed by the chain entanglement of chitosan in PANa soaking. Based on the synergistic effect of dynamic chain entanglement and strong hydrogen bonding, the homogeneous network hydrophobic hydrogel exhibited excellent antiswelling and water-retention capabilities and desirable mechanical properties, demonstrating promising prospect in both air and aquatic conditions. Furthermore, the well-ordered hydrophobic structure induced by electrostatic interactions endowed the hydrogel with high stretchability (1500%), high toughness (2.4 $MJ{\cdot}m^{-3}$), and excellent elastic recovery behavior (elastic recovery ratio of 95%). Considering the superior functionalities mentioned above as well as the excellent electromechanical performance, the hydrogel was appropriate for fabricating wearable sensors for human activity detection and health management. Additionally, thanks to the stable electrical sensitivity in an aquatic environment (GF = 1.45), a transparent hydrogel-based device for underwater communication was assembled to transmit information through Morse codes. This optical transparent hydrogel sensor also showed significant application potential in wearable bioelectronics and bionic skins such as electrodes in wireless ECG monitoring modules. Our research on multiple dynamic interacted HA hydrogels paves the way for constructing intelligent soft materials applied in harsh environments.

EXPERIMENTAL SECTION

Synthesis of HA Hydrogel. The HA hydrogel was prepared by in situ free radical polymerization between hydrophilic monomers and hydrophobic micelles in the presence of chitosan. Typically, MMA (1.18 mL) was dissolved in 20 mL of deionized water with CTAB (3.0 g) at 50 °C under magnetic stirring. After the bubbles disappeared and a transparent micelle dispersion formed, AA (1 mL) and HEAA (10.69 mL) were added into the mixture when it cooled to room temperature. Subsequently, 0.3 g of chitosan encountered the microemulsion under ultrasonic radiation. Afterward, 36 mg of AIBA as the thermal initiator was mixed and homogeneously stirred, followed by pouring the precursor into a customized mold. Finally, the HA hydrogel was obtained after one-pot polymerization at 50 °C for 6 h. As comparison, similar steps were followed to prepare a hydrogel in the absence of chitosan according to the composition in Table S1.

Preparation of the Electrostatically Interacting HA Hydrogel. The as-prepared HA hydrogel was immersed into a series of PANa solutions (mass concentrations of 18.11, 36.22, and 54.34%) for different times to obtain the electrostatically interacting HA hydrogel. After a soaking process for 45 min, the chitosan formed efficacious chain entanglement in a saturated PANa solution.

Characterizations. The chemical structure of the raw materials and the hydrogels was recorded by ATR−FTIR spectra. The XRD and ATR−FTIR spectra were collected to prove the composition and physical interactions in the materials. The optical transparency of the hydrogels was measured in quartz cells by a UV−vis spectrophotometer at room temperature. Furthermore, the SEM equipped with

https://doi.org/10.1021/acs.chemmater.3c02454
Chem. Mater. XXXX, XXX, XXX−XXX

the EDS was conducted to investigate the microstructure of the lyophilized cross-sections of hydrogels.

For the mechanical performance, a universal mechanical test machine was used to record the results of the tensile property test and loading−unloading tests. The corresponding calculation of energy dissipation coefficient and elastic recovery ratio were presented according to the procedure described in a previous study.[61] A rheometer was applied to analyze the viscoelastic behavior of the materials at varying angular frequencies and strains. Besides, the lap-shear test by a universal mechanical machine was performed to test the adhesiveness of the hydrogel both in air and underwater environment. The swelling ratio and water retention were characterized by testing the residual weight of the disk samples in deionized water and ambient storage, respectively.

The electromechanical properties, especially the relative resistance of the hydrogel, were measured by an inductance, capacitance, and resistance (LCR) meter. Therefore, the electric performance of the fabricated sensor was evaluated using the LCR meter in terrestrial and aquatic environments. The wireless ECG monitoring was realized by assembling the hydrogel electrode into an AD8232 module.

The details on materials and methods are shown in the Supporting Information.

■ ASSOCIATED CONTENT

Supporting Information

The Supporting Information is available free of charge at https://pubs.acs.org/doi/10.1021/acs.chemmater.3c02454.

Materials and methods; SEM images and XPS spectrum of the deconvoluted C 1s orbit of PANa, and N 1s orbit of the contrast hydrogels; XRD profile of the prepared HA hydrogel after immersion in PANa solution; small-angle X-ray scattering intensity profiles of the HA hydrogels; tensile curves of the contrast hydrogels; dissipated energy in consecutive loading−unloading tests of the HA hydrogel and the electrostatically interacting HA hydrogels in air and underwater; tensile strain curve of the HA hydrogels soaked for different concentrations and time; comparison strain curve of HA hydrogel with different MMA concentrations; consecutive loading−unloading test with resting intervals of the HA hydrogels; calculated hysteresis ratios of the hydrogels; stress relaxation behavior of HA hydrogels; adhesion strength−displacement curves in amphibious scenario and related pictures; antidehydration performances; zeta potential of the HA hydrogel precursors; WCA results of the hydrogels; conductivity of the as-prepared hydrogels; schematic illustration of underwater sensing and real-time relative resistance variation for subtle strain; ECG monitoring by the commercial electrode; and composition of the hydrogels (PDF)

The luminance variation of an LED with stretching in air and underwater (MP4)

Underwater adhesion of the hydrogel to diverse substrates (MP4)

■ AUTHOR INFORMATION

Corresponding Authors

Yu-I Hsu − *Department of Applied Chemistry, Osaka University, Suita, Osaka 565-0871, Japan;* orcid.org/0000-0002-4533-7200; Email: yuihsu@chem.eng.osaka-u.ac.jp

Hiroshi Uyama − *Department of Applied Chemistry, Osaka University, Suita, Osaka 565-0871, Japan;* orcid.org/0000-0002-8587-2507; Email: uyama@chem.eng.osaka-u.ac.jp

Authors

Peng Du − *Department of Applied Chemistry, Osaka University, Suita, Osaka 565-0871, Japan;* orcid.org/0009-0005-8661-2044

Juan Wang − *Department of Applied Chemistry, Osaka University, Suita, Osaka 565-0871, Japan*

Complete contact information is available at: https://pubs.acs.org/10.1021/acs.chemmater.3c02454

Notes

The authors declare no competing financial interest.

■ ACKNOWLEDGMENTS

This work was supported by the Japan Society for the Promotion of Science (JSPS) KAKENHI Grants (no. 20H02797), Japan Science and Technology Agency (JST) (Grant Number JPMJPF2218), and JST PRESTO (Grant Number JPMJPR23N4). P.D. and J.W. acknowledge the support from the China Scholarship Council (CSC), China and the Ministry of Education, Culture, Sports, Science and Technology (MEXT), Japan via a scholarship grant.

■ REFERENCES

(1) Ates, H. C.; Nguyen, P. Q.; Gonzalez-Macia, L.; Morales-Narváez, E.; Güder, F.; Collins, J. J.; Dincer, C. End-to-End Design of Wearable Sensors. *Nat. Rev. Mater.* **2022**, *7*, 887−907.

(2) Kim, S.; Baek, S.; Sluyter, R.; Konstantinov, K.; Kim, J. H.; Kim, S.; Kim, Y. H. Wearable and Implantable Bioelectronics as Eco-Friendly and Patient-Friendly Integrated Nanoarchitectonics for Next-Generation Smart Healthcare Technology. *EcoMat* **2023**, *5*, No. e12356.

(3) Song, Y.; Min, J.; Yu, Y.; Wang, H.; Yang, Y.; Zhang, H.; Gao, W. Wireless Battery-Free Wearable Sweat Sensor Powered by Human Motion. *Sci. Adv.* **2020**, *6*, No. eaay9842.

(4) Wang, S.; Gao, Y.; Wei, A.; Xiao, P.; Liang, Y.; Lu, W.; Chen, C.; Zhang, C.; Yang, G.; Yao, H.; et al. Asymmetric Elastoplasticity of Stacked Graphene Assembly Actualizes Programmable Untethered Soft Robotics. *Nat. Commun.* **2020**, *11*, 4359.

(5) Li, J.; Jia, H.; Zhou, J.; Huang, X.; Xu, L.; Jia, S.; Gao, Z.; Yao, K.; Li, D.; Zhang, B.; et al. Thin, Soft, Wearable System for Continuous Wireless Monitoring of Artery Blood Pressure. *Nat. Commun.* **2023**, *14*, 5009.

(6) Tutika, R.; Haque, A. B. M. T.; Bartlett, M. D. Self-Healing Liquid Metal Composite for Reconfigurable and Recyclable Soft Electronics. *Commun. Mater.* **2021**, *2*, 64.

(7) Yu, D.; Liao, Y.; Song, Y.; Wang, S.; Wan, H.; Zeng, Y.; Yin, T.; Yang, W.; He, Z. A Super-Stretchable Liquid Metal Foamed Elastomer for Tunable Control of Electromagnetic Waves and Thermal Transport. *Adv. Sci.* **2020**, *7*, 2000177.

(8) Someya, T.; Sekitani, T.; Iba, S.; Kato, Y.; Kawaguchi, H.; Sakurai, T. A Large-Area, Flexible Pressure Sensor Matrix with Organic Field-Effect Transistors for Artificial Skin Applications. *Proc. Natl. Acad. Sci. U.S.A.* **2004**, *101*, 9966−9970.

(9) Fu, F.; Wang, J.; Zeng, H.; Yu, J. Functional Conductive Hydrogels for Bioelectronics. *ACS Mater. Lett.* **2020**, *2*, 1287−1301.

(10) Feig, V. R.; Tran, H.; Lee, M.; Bao, Z. Mechanically Tunable Conductive Interpenetrating Network Hydrogels That Mimic the Elastic Moduli of Biological Tissue. *Nat. Commun.* **2018**, *9*, 2740.

(11) Zhu, T.; Ni, Y.; Biesold, G. M.; Cheng, Y.; Ge, M.; Li, H.; Huang, J.; Lin, Z.; Lai, Y. Recent Advances in Conductive Hydrogels: Classifications, Properties, and Applications. *Chem. Soc. Rev.* **2023**, *52*, 473−509.

(12) Wang, S.; Li, S.; Wang, H.; Lu, H.; Zhu, M.; Wu, X.-E.; Liang, H.; Liang, X.; Zhang, Y. Highly Adhesive Epidermal Sensors with Superior Water-Interference-Resistance for Aquatic Applications. *Adv. Funct. Mater.* **2023**, *33*, 2302687.
(13) Fan, H.; Wang, J.; Gong, J. P. Barnacle Cement Proteins-Inspired Tough Hydrogels with Robust, Long-Lasting, and Repeatable Underwater Adhesion. *Adv. Funct. Mater.* **2021**, *31*, 2009334.
(14) Xu, J.; Jin, R.; Ren, X.; Gao, G. Cartilage-Inspired Hydrogel Strain Sensors with Ultrahigh Toughness, Good Self-Recovery and Stable Anti-Swelling Properties. *J. Mater. Chem. A* **2019**, *7*, 25441−25448.
(15) Luo, Y.; Abidian, M. R.; Ahn, J.-H.; Akinwande, D.; Andrews, A. M.; Antonietti, M.; Bao, Z.; Berggren, M.; Berkey, C. A.; Bettinger, C. J.; et al. Technology Roadmap for Flexible Sensors. *ACS Nano* **2023**, *17*, 5211−5295.
(16) Wei, J.; Xiao, P.; Chen, T. Water-Resistant Conductive Gels toward Underwater Wearable Sensing. *Adv. Mater.* **2023**, *35*, 2211758.
(17) Wei, J.; Zheng, Y.; Chen, T. A Fully Hydrophobic Ionogel Enables Highly Efficient Wearable Underwater Sensors and Communicators. *Mater. Horiz.* **2021**, *8*, 2761−2770.
(18) Jiang, H.; Duan, L.; Ren, X.; Gao, G. Hydrophobic Association Hydrogels with Excellent Mechanical and Self-Healing Properties. *Eur. Polym. J.* **2019**, *112*, 660−669.
(19) Yang, H.; Lu, H.; Miao, Y.; Cong, Y.; Ke, Y.; Wang, J.; Yang, H.; Fu, J. Non-Swelling, Super-Tough, Self-Healing, and Multi-Responsive Hydrogels Based on Micellar Crosslinking for Smart Switch and Shape Memory. *Chem. Eng. J.* **2022**, *450*, 138346.
(20) Wang, S.; Wang, L.; Qu, X.; Lei, B.; Zhao, Y.; Wang, Q.; Wang, W.; Shao, J.; Dong, X. Ultrasonic-Induced Synthesis of Underwater Adhesive and Antiswelling Hydrogel for Strain Sensor. *ACS Appl. Mater. Interfaces* **2022**, *14*, 50256−50265.
(21) Guo, H.; Nakajima, T.; Hourdet, D.; Marcellan, A.; Creton, C.; Hong, W.; Kurokawa, T.; Gong, J. P. Hydrophobic Hydrogels with Fruit-Like Structure and Functions. *Adv. Mater.* **2019**, *31*, 1900702.
(22) Wu, J.; Pan, Z.; Zhao, Z.-Y.; Wang, M.-H.; Dong, L.; Gao, H.-L.; Liu, C.-Y.; Zhou, P.; Chen, L.; Shi, C.-J.; et al. Anti-Swelling, Robust, and Adhesive Extracellular Matrix-Mimicking Hydrogel Used as Intraoral Dressing. *Adv. Mater.* **2022**, *34*, 2200115.
(23) Khan, M.; Shah, L. A.; Ara, L.; Ullah, R.; Yoo, H.-M. Micelle-Micelle Cross-Linked Highly Stretchable Conductive Hydrogels for Potential Applications of Strain and Electronic Skin Sensors. *Chem. Mater.* **2023**, *35*, 5582−5592.
(24) Long, J. A.; Rankin, B. M.; Ben-Amotz, D. Micelle Structure and Hydrophobic Hydration. *J. Am. Chem. Soc.* **2015**, *137*, 10809−10815.
(25) Mihajlovic, M.; Wyss, H. M.; Sijbesma, R. P. Effects of Surfactant and Urea on Dynamics and Viscoelastic Properties of Hydrophobically Assembled Supramolecular Hydrogel. *Macromolecules* **2018**, *51*, 4813−4820.
(26) Tuncaboylu, D. C.; Sahin, M.; Argun, A.; Oppermann, W.; Okay, O. Dynamics and Large Strain Behavior of Self-Healing Hydrogels with and without Surfactants. *Macromolecules* **2012**, *45*, 1991−2000.
(27) Qi, C.; Dong, Z.; Huang, Y.; Xu, J.; Lei, C. Tough, Anti-Swelling Supramolecular Hydrogels Mediated by Surfactant-Polymer Interactions for Underwater Sensors. *ACS Appl. Mater. Interfaces* **2022**, *14*, 30385−30397.
(28) Tuncaboylu, D. C.; Sari, M.; Oppermann, W.; Okay, O. Tough and Self-Healing Hydrogels Formed via Hydrophobic Interactions. *Macromolecules* **2011**, *44*, 4997−5005.
(29) Cai, Y.; Wan, K.; Chen, Q.; Hong, M.; Zhou, Z.-X.; Fu, H. Anti-Swelling Hydrogels Based on Surfactant-Polymer Interactions for Underwater Sensing with Excellent Mechanical Properties. *J. Mater. Chem. C* **2023**, *11*, 12981−12991.
(30) Ni, Y.; Zang, X.; Chen, J.; Zhu, T.; Yang, Y.; Huang, J.; Cai, W.; Lai, Y. Flexible Mxene-Based Hydrogel Enables Wearable Human-Computer Interaction for Intelligent Underwater Communication and Sensing Rescue. *Adv. Funct. Mater.* **2023**, *33*, 2301127.
(31) Huang, G.; Tang, Z.; Peng, S.; Zhang, P.; Sun, T.; Wei, W.; Zeng, L.; Guo, H.; Guo, H.; Meng, G. Modification of Hydrophobic Hydrogels into a Strongly Adhesive and Tough Hydrogel by Electrostatic Interaction. *Macromolecules* **2022**, *55*, 156−165.
(32) Zhao, Y.; Song, S.; Ren, X.; Zhang, J.; Lin, Q.; Zhao, Y. Supramolecular Adhesive Hydrogels for Tissue Engineering Applications. *Chem. Rev.* **2022**, *122*, 5604−5640.
(33) Huang, G.; Guo, H.; Tang, Z.; Peng, S.; Liang, H.; Meng, G.; Zhang, P. Tough Hydrophobic Hydrogels for Monitoring Human Moderate Motions in Both Air and Underwater Environments. *Chem. Mater.* **2023**, *35*, 5953−5962.
(34) Demott, C. J.; Jones, M. R.; Chesney, C. D.; Yeisley, D. J.; Culibrk, R. A.; Hahn, M. S.; Grunlan, M. A. Ultra-High Modulus Hydrogels Mimicking Cartilage of the Human Body. *Macromol. Biosci.* **2022**, *22*, 2200283.
(35) Zhao, H.; Hao, S.; Fu, Q.; Zhang, X.; Meng, L.; Xu, F.; Yang, J. Ultrafast Fabrication of Lignin-Encapsulated Silica Nanoparticles Reinforced Conductive Hydrogels with High Elasticity and Self-Adhesion for Strain Sensors. *Chem. Mater.* **2022**, *34*, 5258−5272.
(36) Liu, X.; Zhang, Q.; Gao, G. Solvent-Resistant and Nonswellable Hydrogel Conductor toward Mechanical Perception in Diverse Liquid Media. *ACS Nano* **2020**, *14*, 13709−13717.
(37) Dou, X.; Wang, H.; Yang, F.; Shen, H.; Wang, X.; Wu, D. One-Step Soaking Strategy toward Anti-Swelling Hydrogels with a Stiff "Armor. *Adv. Sci.* **2023**, *10*, 2206242.
(38) Du, P.; Wang, J.; Hsu, Y.-I; Uyama, H. Bio-Inspired Homogeneous Conductive Hydrogel with Flexibility and Adhesiveness for Information Transmission and Sign Language Recognition. *ACS Appl. Mater. Interfaces* **2023**, *15*, 23711−23724.
(39) Pan, L.; Yu, G.; Zhai, D.; Lee, H. R.; Zhao, W.; Liu, N.; Wang, H.; Tee, B. C. K.; Shi, Y.; Cui, Y.; et al. Hierarchical Nanostructured Conducting Polymer Hydrogel with High Electrochemical Activity. *Proc. Natl. Acad. Sci. U.S.A.* **2012**, *109*, 9287−9292.
(40) Zhang, Q.; Liu, X.; Zhang, J.; Duan, L.; Gao, G. A Highly Conductive Hydrogel Driven by Phytic Acid towards a Wearable Sensor with Freezing and Dehydration Resistance. *J. Mater. Chem. A* **2021**, *9*, 22615−22625.
(41) Zhang, S.; Li, Y.; Zhang, H.; Wang, G.; Wei, H.; Zhang, X.; Ma, N. Bioinspired Conductive Hydrogel with Ultrahigh Toughness and Stable Antiswelling Properties for Articular Cartilage Replacement. *ACS Mater. Lett.* **2021**, *3*, 807−814.
(42) Kumar, M. N. V. R.; Muzzarelli, R. A. A.; Muzzarelli, C.; Sashiwa, H.; Domb, A. J. Chitosan Chemistry and Pharmaceutical Perspectives. *Chem. Rev.* **2004**, *104*, 6017−6084.
(43) Yang, Y.; Wang, X.; Yang, F.; Wang, L.; Wu, D. Highly Elastic and Ultratough Hybrid Ionic-Covalent Hydrogels with Tunable Structures and Mechanics. *Adv. Mater.* **2018**, *30*, 1707071.
(44) Xu, L.; Wang, C.; Cui, Y.; Li, A.; Qiao, Y.; Qiu, D. Conjoined-Network Rendered Stiff and Tough Hydrogels from Biogenic Molecules. *Sci. Adv.* **2019**, *5*, No. eaau3442.
(45) He, S.; Guo, B.; Sun, X.; Shi, M.; Zhang, H.; Yao, F.; Sun, H.; Li, J. Bio-Inspired Instant Underwater Adhesive Hydrogel Sensors. *ACS Appl. Mater. Interfaces* **2022**, *14*, 45869−45879.
(46) Xiang, L.; Gong, L.; Zhang, J.; Zhang, L.; Hu, W.; Wang, W.; Lu, Q.; Zeng, H. Probing Molecular Interactions of Pegylated Chitosan in Aqueous Solutions Using a Surface Force Apparatus. *Phys. Chem. Chem. Phys.* **2019**, *21*, 20571−20581.
(47) Cui, C.; Shao, C.; Meng, L.; Yang, J. High-Strength, Self-Adhesive, and Strain-Sensitive Chitosan/Poly(acrylic acid) Double-Network Nanocomposite Hydrogels Fabricated by Salt-Soaking Strategy for Flexible Sensors. *ACS Appl. Mater. Interfaces* **2019**, *11*, 39228−39237.
(48) Chen, J.; Peng, Q.; Thundat, T.; Zeng, H. Stretchable, Injectable, and Self-Healing Conductive Hydrogel Enabled by Multiple Hydrogen Bonding toward Wearable Electronics. *Chem. Mater.* **2019**, *31*, 4553−4563.
(49) Mihajlovic, M.; Staropoli, M.; Appavou, M.-S.; Wyss, H. M.; Pyckhout-Hintzen, W.; Sijbesma, R. P. Tough Supramolecular

https://doi.org/10.1021/acs.chemmater.3c02454
Chem. Mater. XXXX, XXX, XXX−XXX

Hydrogel Based on Strong Hydrophobic Interactions in a Multiblock Segmented Copolymer. *Macromolecules* **2017**, *50*, 3333−3346.
(50) Senra, T. D. A.; Khoukh, A.; Desbrières, J. Interactions between Quaternized Chitosan and Surfactant Studied by Diffusion NMR and Conductivity. *Carbohydr. Polym.* **2017**, *156*, 182−192.
(51) Kong, W.; Wang, C.; Jia, C.; Kuang, Y.; Pastel, G.; Chen, C.; Chen, G.; He, S.; Huang, H.; Zhang, J.; et al. Muscle-Inspired Highly Anisotropic, Strong, Ion-Conductive Hydrogels. *Adv. Mater.* **2018**, *30*, 1801934.
(52) Sun, Z.; Dong, C.; Chen, B.; Li, W.; Hu, H.; Zhou, J.; Li, C.; Huang, Z. Strong, Tough, and Anti-Swelling Supramolecular Conductive Hydrogels for Amphibious Motion Sensors. *Small* **2023**, *19*, 2303612.
(53) Cao, M.; Liu, B.-W.; Zhang, L.; Peng, Z.-C.; Zhang, Y.-Y.; Wang, H.; Zhao, H.-B.; Wang, Y.-Z. Fully Biomass-Based Aerogels with Ultrahigh Mechanical Modulus, Enhanced Flame Retardancy, and Great Thermal Insulation Applications. *Composites, Part B* **2021**, *225*, 109309.
(54) Zhang, H.; Zhu, S.; Yang, J.; Ma, A.; Chen, W. Enhanced Removal Efficiency of Heavy Metal Ions by Assembling Phytic Acid on Polyamide Nanofiltration Membrane. *J. Membr. Sci.* **2021**, *636*, 119591.
(55) Aleid, S.; Wu, M.; Li, R.; Wang, W.; Zhang, C.; Zhang, L.; Wang, P. Salting-in Effect of Zwitterionic Polymer Hydrogel Facilitates Atmospheric Water Harvesting. *ACS Mater. Lett.* **2022**, *4*, 511−520.
(56) Li, J.; Li, J.; Tang, Y.; Liu, Z.; Zhang, Z.; Wu, H.; Shen, B.; Su, M.; Liu, M.; Li, F. Touchable Gustation via a Hoffmeister Gel Iontronic Sensor. *ACS Nano* **2023**, *17*, 5129−5139.
(57) Wang, Z.; Chen, J.; Cong, Y.; Zhang, H.; Xu, T.; Nie, L.; Fu, J. Ultrastretchable Strain Sensors and Arrays with High Sensitivity and Linearity Based on Super Tough Conductive Hydrogels. *Chem. Mater.* **2018**, *30*, 8062−8069.
(58) Zhang, K.; Zhang, X.; Fang, Y.-J.; Cai, J. Strong and Tough Chitosan Aerogels *via* Hofmeister Effect. *Acta Polym. Sin.* **2023**, *54*, 731−740.
(59) Shen, K.; Xu, K.; Zhang, M.; Yu, J.; Yang, Y.; Zhao, X.; Zhang, Q.; Wu, Y.; Zhang, Y.; Cheng, Y. Multiple Hydrogen Bonds Reinforced Conductive Hydrogels with Robust Elasticity and Ultra-Durability as Multifunctional Ionic Skins. *Chem. Eng. J.* **2023**, *451*, 138525.
(60) Mehdizadeh, M.; Weng, H.; Gyawali, D.; Tang, L.; Yang, J. Injectable Citrate-Based Mussel-Inspired Tissue Bioadhesives with High Wet Strength for Sutureless Wound Closure. *Biomaterials* **2012**, *33*, 7972−7983.
(61) Lan, M. H.; Guan, X.; Zhu, D. Y.; Chen, Z. P.; Liu, T.; Tang, Z. Highly Elastic, Self-Healing, Recyclable Interlocking Double-Network Liquid-Free Ionic Conductive Elastomers via Facile Fabrication for Wearable Strain Sensors. *ACS Appl. Mater. Interfaces* **2023**, *15*, 19447−19458.
(62) Gao, Y.; Gu, S.; Duan, L.; Wang, Y.; Gao, G. Robust and Anti-Fatigue Hydrophobic Association Hydrogels Assisted by Titanium Dioxide for Photocatalytic Activity. *Soft Matter* **2019**, *15*, 3897−3905.
(63) Chen, J.; An, R.; Han, L.; Wang, X.; Zhang, Y.; Shi, L.; Ran, R. Tough Hydrophobic Association Hydrogels with Self-Healing and Reforming Capabilities Achieved by Polymeric Core-Shell Nanoparticles. *Mater. Sci. Eng., C* **2019**, *99*, 460−467.
(64) Ling, Q.; Liu, W.; Liu, J.; Zhao, L.; Ren, Z.; Gu, H. Highly Sensitive and Robust Polysaccharide-Based Composite Hydrogel Sensor Integrated with Underwater Repeatable Self-Adhesion and Rapid Self-Healing for Human Motion Detection. *ACS Appl. Mater. Interfaces* **2022**, *14*, 24741−24754.
(65) Pan, M.; Shui, T.; Zhao, Z.; Li, M.; Fan, H.; Wu, J.; Zeng, H. Orchestrating Asymmetric Surface Functionalities on Hydrogel Stamps Where Adhesion Meets Lubrication. *Chem. Mater.* **2023**, *35*, 4998−5008.
(66) Pi, M.; Qin, S.; Wen, S.; Wang, Z.; Wang, X.; Li, M.; Lu, H.; Meng, Q.; Cui, W.; Ran, R. Rapid Gelation of Tough and Anti-Swelling Hydrogels under Mild Conditions for Underwater Communication. *Adv. Funct. Mater.* **2023**, *33*, 2210188.
(67) Zhao, Y.; Wang, F.; Liu, J.; Gan, D.; Lei, B.; Shao, J.; Wang, W.; Wang, Q.; Dong, X. Underwater Self-Healing and Recyclable Ionogel Sensor for Physiological Signal Monitoring. *ACS Appl. Mater. Interfaces* **2023**, *15*, 28664−28674.
(68) Ma, Z.; Bourquard, C.; Gao, Q.; Jiang, S.; De Iure-Grimmel, T.; Huo, R.; Li, X.; He, Z.; Yang, Z.; Yang, G.; et al. Controlled Tough Bioadhesion Mediated by Ultrasound. *Science* **2022**, *377*, 751−755.
(69) Ren, J.; Liu, Y.; Wang, Z.; Chen, S.; Ma, Y.; Wei, H.; Lü, S. An Anti-Swellable Hydrogel Strain Sensor for Underwater Motion Detection. *Adv. Funct. Mater.* **2022**, *32*, 2107404.
(70) Yao, X.; Zhang, S.; Qian, L.; Wei, N.; Nica, V.; Coseri, S.; Han, F. Super Stretchable, Self-Healing, Adhesive Ionic Conductive Hydrogels Based on Tailor-Made Ionic Liquid for High-Performance Strain Sensors. *Adv. Funct. Mater.* **2022**, *32*, 2204565.
(71) Su, G.; Zhang, Y.; Zhang, X.; Feng, J.; Cao, J.; Zhang, X.; Zhou, T. Soft yet Tough: A Mechanically and Functionally Tissue-Like Organohydrogel for Sensitive Soft Electronics. *Chem. Mater.* **2022**, *34*, 1392−1402.
(72) Chen, F.; Zhuang, Q.; Ding, Y.; Zhang, C.; Song, X.; Chen, Z.; Zhang, Y.; Mei, Q.; Zhao, X.; Huang, Q.; et al. Wet-Adaptive Electronic Skin. *Adv. Mater.* **2023**, *35*, 2305630.

https://doi.org/10.1021/acs.chemmater.3c02454
Chem. Mater. XXXX, XXX, XXX−XXX